PAPER

Model for the dependence of cathode voltage in a Hall thruster on facility pressure

View the article online for updates and enhancements.

Model for the dependence of cathode voltage in a Hall thruster on facility pressure

B A Jorns[*] and M P Byrne

Department of Aerospace Engineering, University of Michigan, Ann Arbor, MI 48109, United States of America

E-mail: bjorns@umich.edu

Abstract
An analytical model for the dependence of the cathode coupling voltage in a Hall thruster on facility pressure is derived and investigated. The expression for the coupling voltage is determined by performing a line integral of the generalized Ohm's law from the cathode emitter to the thruster's main plume. The effects of pressure as well as non-classical resistance due to ion acoustic turbulence are included. The resulting model is applied to datasets from 12 different Hall thruster configurations and is shown in all cases to match the trends in the data within experimental uncertainty. The model in turn is used to extrapolate the experimental datasets to on-orbit conditions, and the confidence in these predictions is quantified through the lens of Bayesian parameter estimation. The derived model is discussed in the context of the underlying assumptions as well as previous models that have been proposed for this facility effect.

Keywords: Hall thruster, electric propulsion, facility effects, hollow cathode

(Some figures may appear in colour only in the online journal)

1. Introduction

The problem of facility effects in Hall thruster testing poses a critical challenge for the future development of this technology. The evaluation and qualification of these systems for flight requires a ground-based test environment capable of maintaining a high quality vacuum. While there are a number of facilities that historically have been available for this purpose [1], there are aspects of ground tests—such as the presence of finite background gas and electrically conducting walls—that are known to impact assessments of lifetime, performance, and stability [1–32]. This raises the possibility that ground test results may not be representative of on-orbit behavior.

In light of this operational risk, there are a number of techniques and methodologies that have been proposed to correct for facility effects. Most commonly, to compensate for the presence of residual background gas in the facility [4, 6, 11, 14, 15, 17, 20, 26], operators will measure key aspects

of the thruster operation while systematically decreasing the facility pressure to the lowest value achievable. A function then will be fit to this dataset and extrapolated to zero background pressure. While simple in principle, the challenge in this approach lies in identifying which function is appropriate to use to fit the data and make the extrapolation.

Model selection to date largely has been empirically-driven—informed by the shape of the trends in data—with proposed models varying in complexity from linear [4, 6, 11, 14, 17, 20] to transcendental functions [15]. While most of these proposed functions have been shown to yield agreement with datasets over the measured domain, the fact that these models are empirical raises concerns about their validity outside the range of the experimental data. For example, transcendental functions may match a given dataset with a high degree of accuracy [15], but these functions may not correctly describe physical trends at pressures lower than can be achieved in the facility. If this is the case, the highly nonlinear nature of this function could lead to large errors in the extrapolation to orbit.

---

[*] Author to whom any correspondence should be addressed.

The problem of extrapolation error that stems from model selection in principle could be overcome by rooting fitting functions in a physics-based understanding of the facility effects [19, 30–33]. This ensures that the model will be extensible outside the dataset against which it is matched. The challenge in applying this physics-based approach to date, however, has been that the fundamental processes driving many facility effects are insufficiently understood to derive appropriate fitting models.

The cathode coupling voltage's response to facility pressure is a notable example of a facility effect with poorly understood governing processes. The cathode coupling voltage is the increase in electrical potential from the hollow cathode, the electron source for the thruster, to the plume of the main discharge. It has a direct bearing on the efficiency and overall thrust. While there have been previous efforts to predict the dependence of this coupling voltage on background pressure [19, 30, 31, 33], the physics-based modeling of this facility effect has proved difficult to date. This largely stems from the challenge in self-consistently representing non-classical processes in the cathode plume that are known to impact the electron resistivity [34–43].

With that said, recent experimental work has offered new insight into how this electron resistivity might be modeled. It was shown through direct experimental measurements in the cathode plume of a Hall thurster that the non-classical electron dynamics can be described with simplified algebraic expressions that depend on the local plasma properties [42]. The goal of our study is to leverage this experimentally-validated finding to derive and evaluate a simplified, physics-based scaling law for the dependence of cathode coupling voltage on background pressure.

This paper is organized in the following way. In the first section, we present the underlying theory of the model and the governing assumptions. This yields an algebraic expression for the coupling voltage that has three adjustable model parameters. In the second section, we review the method of Bayesian parameter estimation and how this is applied to infer the model parameters from experimental datasets. In the third section, we summarize existing datasets—drawn from previous studies of several different Hall thrusters—of cathode coupling voltage as a function of pressure. For the fourth section, we present the results of applying the model to these datasets including estimates for uncertainty in the model parameters and the extrapolation of the model to space like conditions. In the fifth and final section, we discuss the physical implications of our results, examine the limitations and applications of the model, and compare our findings to previous efforts to model this effect.

2. Theory

2.1. Definition of cathode coupling voltage

We show in figure 1 an image of a Hall thruster and a cross-sectional view of the canonical geometry of the thruster channel. As depicted here, Hall thrusters are comprised of an axisymmetric annular chamber that supports crossed electric
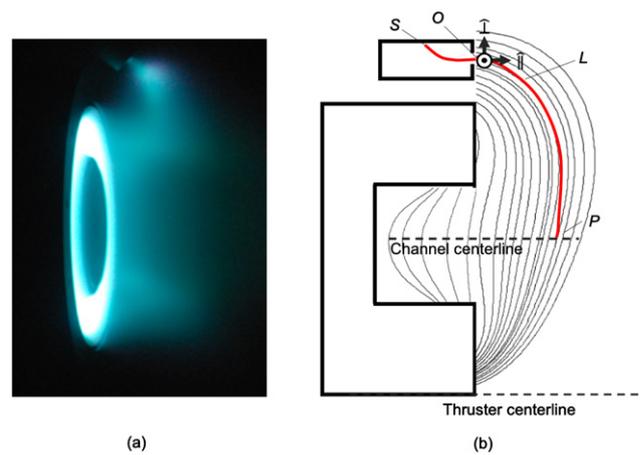

Figure 1. (a) Image of Hall thruster operating with a hollow cathode mounted external to the discharge. (b) Cross-sectional view of Hall thruster channel with notional magnetic field topography and coordinate convention in the near field of the cathode exit.
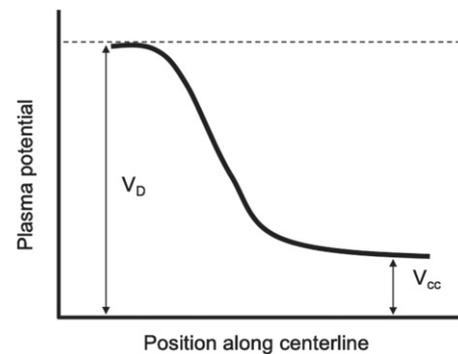

Figure 2. Schematic illustrating the spatial variation of plasma potential along the channel centerline of the Hall thruster.

and magnetic fields. The electric field is provided by a voltage drop of V_D applied between an upstream anode and downstream cathode. Gas flows through the anode to the discharge channel where it is ionized and accelerated downstream by the electric field. The hollow cathode serves as the terminal point for the potential drop as well as the electron source for the Hall thruster. It provides the charge carriers that ionize the propellant in the discharge and neutralize it once it has been expelled.

We show in figure 2 an illustration of the spatial variation of electrical potential along the channel centerline of a Hall thruster. Ions born in the upstream region near the anode accelerate down the potential well and out of the geometry. Ideally, the ions gain a kinetic energy equivalent to the total potential drop, V_D. In practice, however, only a fraction of the potential is available for this process [44]. A portion of the accelerating voltage, the so-called cathode coupling voltage, V_{cc}, is devoted to drawing electrons out of the cathode and into the main discharge. This electric potential does not contribute to the acceleration of the propellant and consequently lowers the generated thrust [44, 45]. It is in this way that variations in the cathode coupling voltage with facility pressure can result in changes in overall thruster performance.

2.2. Application of generalized Ohm's law to cathode plume

To motivate a model for the dependence of cathode coupling voltage on facility pressure, we consider the canonical geometry in figure 1(b) where we show the 2D plane the cathode shares with the thruster mid-plane. As illustrated here, the cathode plasma environment is subject to an applied magnetic field originating from the thruster body. We use this field to define a coordinate convention where $\hat{\parallel}$ denotes the local direction parallel to the magnetic field, $\hat{\perp}$ is perpendicular to the field, and $\hat{\parallel} \times \hat{\perp}$ is the cross-field direction, out of the plane.

The generalized Ohm's law for the electrons in this plane is given by

$$\vec{E} = \bar{\bar{\eta}} \cdot \vec{j}_e - \frac{1}{q n_e} \nabla \left[T_e n_e \right], \tag{1}$$

where $\vec{E}$ denotes the local electric field, $\vec{j}_e$ is the electron current density in the plane, q is fundamental charge, n_e is the electron density, T_e is the electron temperature in units of energy and $\bar{\bar{\eta}}$ is a resistivity tensor of the plasma. By symmetry, we make the assumption that we can neglect electric fields and pressure gradients in the $\hat{\parallel} \times \hat{\perp}$ direction. We therefore have in the thruster mid-plane $\vec{j}_e = (j_{e(\parallel)}, j_{e(\perp)})$, and the resistivity tensor becomes

$$\bar{\bar{\eta}} = \frac{m_e}{q^2 n_e} \begin{pmatrix} \nu_{e(\parallel)} & 0 \\ 0 & \nu_{e(\perp)} + \frac{q^2 B_0^2}{m_e^2 \nu_{e(\parallel \times \perp)}} \end{pmatrix}, \tag{2}$$

where $\nu_{e()}$ denotes the effective electron collision frequency acting on the species in each direction and B_0 is the magnitude of the magnetic field. The anisotropic nature of the resistivity stems from the fact that the electron dynamics and the effective drag induced on this species by collisional or non-classical effects varies depending on the direction with respect to the magnetic field [42].

We find the cathode coupling potential by integrating equation (1) along a line segment (red line in figure 1(b)) that begins at the cathode surface, denoted point S, passes through the cathode orifice, denoted point 0, and connects to the main discharge plume of the thruster at point P. This yields

$$V_{cc} = V_{int} + V_{plume}$$

$$V_{int} = \int_S^0 \left(-\bar{\bar{\eta}} \cdot \vec{j}_e + \frac{1}{q n_e} \nabla \left[T_e n_e \right] \right) \cdot d\vec{r}$$

$$V_{plume} = \int_0^P \left(-\bar{\bar{\eta}} \cdot \vec{j}_e + \frac{1}{q n_e} \nabla \left[T_e n_e \right] \right) \cdot d\vec{r}, \tag{3}$$

where we have divided the path integral into two contributions. V_{int} denotes the voltage change from the line integral inside the cathode to the exit orifice. It is the voltage necessary to draw the current from the internal cathode emitter out into the cathode plume. As the neutral density inside the cathode and its orifice are several orders of magnitude higher than the changes in neutral density that result from varying facility pressure, we assume that V_{int} is independent of this facility effect. V_{plume} is the potential change along the segment from the cathode exit to the main plume. This is the potential that drives electrons

to connect to the main discharge. Since the neutral and plasma density originating from the cathode decrease precipitously as the plume expands from the orifice, we assume V_{plume} will be susceptible to changes in facility pressure. Our subsequent discussion thus focuses on this term.

To motivate an expression for V_{plume}, we invoke two key assumptions. First, we assume that the electrons are isothermal. The approximate isothermality of the cathode plume has been remarked upon in previous experimental studies of hollow cathodes in a Hall thruster [37, 42] and is frequently invoked in the model of thruster far-field plumes [46]. Second, we introduce a demarcation between the near-field and far-field of the cathode plume, denoted point L, where we assume the far-field region is current free. This is consistent with the treatment of previous simplified far-field plume models [46] and derivations of scaling laws [31]. Subject to these two assumptions, we can express the plume cathode coupling voltage from equation (3) as

$$V_{plume} = V_{resistive} + V_{Boltzmann}$$

$$V_{resistive} = -\int_0^L \left(\bar{\bar{\eta}} \cdot \vec{j}_e \right) \cdot d\vec{r}$$

$$V_{Boltzmann} = -T_e \, \ln \left(\frac{n_{e(0)}}{n_{e(P)}} \right), \tag{4}$$

where $n_{e(0)}$ is the electron density at the exit of the cathode and $n_{e(P)}$ is the electron density at the connection point to the main plume. Here we have introduced $V_{resistive}$, which represents the voltage increase that stems from electrical resistance as current flows through the near-field plasma. The second term, $V_{Boltzmann}$, is the Boltzmann contribution to the change in potential that is the consequence of the variation in density from the cathode exit to the connection point in the plume. We motivate in the following expressions for each of these contributions in terms of background plasma properties.

2.3. Boltzmann contribution to cathode coupling voltage

To simplify the Boltzmann term in equation (4), we consider in more detail the contributions to the plasma density at points 0 and P. Following reference [31], there are three sources for the plasma density at the connection point to the plume, $n_{e(P)} = n_{e(P)}^T + n_{e(P)}^C + n_{e(P)}^F$, where $n_{e(P)}^T$ is the contribution of plasma from the thruster main discharge at ideal vacuum conditions, $n_{e(P)}^C$ is from the cathode plasma, and $n_{e(P)}^F$ is the plasma density that results from ionization of neutral background gas in the facility. Given that the cathode plume expands, leading to a precipitous drop in density at point P, we assume that the plasma from the cathode density is negligible compared to the other two components. We therefore approximate $n_{e(P)} \approx n_{e(P)}^T + c' n_B$ where $c' < 1$ is a constant of proportionality and n_B is the background neutral gas density from the facility.

There are also three contributions to the plasma density at the cathode exit (location 0): $n_{e(0)} = n_{e(0)}^T + n_{e(0)}^C + n_{e(0)}^F$. Here $n_{e(0)}^T$ is the density from the thruster main discharge at ideal vacuum conditions, $n_{e(0)}^C$ denotes the contribution from the cathode, and $n_{e(0)}^F$ stems from the plasma density that exists

when there is finite background neutral pressure. As the plasma density at the exit of the cathode is the highest density in the entire thruster, comparable to 10^{18} to 10^{20} m^{-3}, we assume it dominates the other two sources. This allows us to simplify the expression for plasma density at the cathode exit to $n_{e(0)} \approx n_{e(0)}^C$, which is independent of facility pressure.

Armed with these expressions for the densities at P and 0, we can reduce $V_{\text{Boltzmann}}$ in equation (4) to

$$V_{\text{Boltzmann}} = V_{b(0)} + T_e \ln\left(1 + \frac{\bar{P}_B}{\bar{P}_T}\right). \tag{5}$$

Here we have defined a normalized facility pressure $\bar{P}_B = P_B/P_{\text{ref}}$ where P_{ref} is a constant reference value. We also have introduced two constants, $V_{b(0)} = T_e \ln(n_{e(P)}^T/n_{e(0)})$ and $\bar{P}_T = (k_B T_F n_{e(P)}^T)/(c' P_{\text{ref}})$, were T_F is the temperature of facility neutrals and k_B is the Boltzmann constant. The former corresponds to the voltage that results from the Boltzmann effect at zero background pressure. The latter is the ratio at point P of the plasma density originating from the thruster to the plasma density from the facility at the reference pressure. In this form, we see from equation (5) that at zero background pressure, the Boltzmann contribution will be $V_{\text{Boltzmann}} = V_{b(0)} < 0$ since the cathode density will exceed the density of plasma at the connection point P. The coupling voltage then will increase with facility pressure, as captured by the second term. Notably, this is opposite the trend posited by Mikellides *et al* [31] and stems from differences in the assumptions we make about the plasma densities at the locations 0 and P. We return to a discussion of this discrepancy in section 6.

2.4. Resistive contribution to cathode coupling voltage

In order to evaluate the resistive term in equation (4), we choose an integral path that is co-aligned with the local magnetic field. The expression thus can be replaced with an integral with respect to one coordinate, x, that denotes distance along the field line:

$$V_{\text{resistive}} = -\int_0^L \frac{m_e \nu_{e(\parallel)}}{q^2 n_e} j_{e(\parallel)} \, dx. \tag{6}$$

To evaluate this expression, we need to estimate the parallel current density, $j_{e(\parallel)}$, the parallel collision frequency, $\nu_{e(\parallel)}$, and the local electron density, n_e. For the collision frequency, previous work has shown that the electron transport is non-classical in the near-field plume of the hollow cathode [35, 36, 42]. Instead of interparticle collisions, the effective drag on electrons in this direction is dominated by the onset of kinetically-driven ion acoustic turbulence (IAT). References [42, 47] demonstrated experimentally and numerically that the effect of the growth of this IAT can be represented with a simplified expression that depends on the local plasma properties:

$$\nu_{e(\parallel)} = \alpha \omega_{\text{pi}} M_{e(\parallel)}, \tag{7}$$

where ω_{pi} is the ion plasma frequency, $M_e = j_{e(\parallel)}/(n_e q)/v_{te}$ is the parallel electron Mach number, v_{te} is the electron thermal speed, and α is a proportionality constant on order of unity.

To estimate the current density in equation (6), we make the assumption that no current in the near-field is conducted across field lines (in the $\hat{\perp}$ direction). We justify this in the context of equation (2) where we see that for a magnetized plasma, $\eta_\parallel/\eta_\perp \approx (\nu_{e(\parallel)}\nu_{e(\parallel \times \perp)})/\omega_{ce}^2$, where ω_{ce} denotes the electron cyclotron frequency. For the near-field hollow cathode plume, we assume the magnetic field is sufficiently large that $\nu_{e(\parallel \times \perp)}, \nu_{e(\parallel)} \ll \omega_{ce}$. This claim is supported by experimental measurements that have been performed in the cathode plume operating with a Hall thruster [42] and is an assumption employed in high-fidelity cathode plume simulations [38]. In this limit, the resistivity in the parallel direction is negligible compared to the resistivity perpendicular to the applied field, i.e. $\eta_\parallel \ll \eta_\perp$. The current in the near field therefore will flow primarily in the parallel direction, and since the magnetic field lines are all oriented in one direction at this location, we can use electron continuity to make the approximation:

$$j_{e(\parallel)} = I_D/(\pi r^2), \tag{8}$$

where I_D denotes the discharge current, r is the radius of the cathode orifice, and we have neglected ionization in the near-field plume.

For the plasma density in the near field in equation (6), we make the simplification—as is consistent with the 1D models that have been employed to date for cathode plumes—that the plume expands conically [44] from the orifice. We thus can write

$$n_e = \frac{n_{e(0)}}{\left(\frac{x}{r} + \tan\theta\right)^2} + n_{e(c)}, \tag{9}$$

where θ is the half angle of expansion and $n_{e(c)} = n_{e(c)}^T + n_{e(c)}^F$ denotes the plasma density in the plume between points 0 and L originating from sources other than the cathode. Following the discussion in section 2.3, $n_{e(c)}^T$ denotes plasma density originating from the thruster and $n_{e(c)}^F$ is the plasma density from ionization of ambient neutral gas. We again assume this latter density scales linearly with the background neutral density: $n_{e(c)}^F = c'n_B$, where c' is a constant of proportionality.

As a final simplification, we note that for typical properties of the cathode plume, $\tan\theta \approx 1$ and $r/L \ll 1$ (the ratio of cathode exit radius to coupling length). We also recall that the plasma density at the cathode exit plane is higher than the densities that originate from the facility and thruster, $n_{e(0)} \gg n_{e(c)}$. These simplifying assumptions allow us to reduce the expression that results from substituting equations (7)–(9) into equation (6) to

$$V_{\text{resistive}} = V_{\text{plume}(0)}\left(\frac{2}{c_1 + c_2 \bar{P}_B}\right)^2$$

$$\times \left[\frac{2 + c_1 + c_2 \bar{P}_B}{(1 + c_1 + c_2 \bar{P}_B)^{1/2}} - 2\right], \tag{10}$$

where we have introduced a constant with units of voltage:

$$V_{\text{plume}(0)} = \alpha \left(\frac{I_D}{2\pi r^2}\right)^2 \left(\frac{L^4}{r^3}\right) \frac{1}{n_{e(0)}^{3/2}} \frac{m_e}{q^2} \sqrt{\frac{m_e}{q\epsilon_0 m_i T_e}}. \tag{11}$$

This parameter is assumed to be constant as I_D is typically held constant during Hall thruster facility pressure studies. We sim-

ilarly have defined constants given by $c_1 = n_{e(c)}^{T}/n_{e(0)}(L/r)^2 > 0$ and $c_2 = c' P_{ref}/(k_B T_F n_{e(0)})(L/r)^2 > 0$.

Equation (10) shows that the resistive contribution to the coupling voltage monotonically decreases with pressure, and at $\bar{P}_B \to 0$, $V_{resistive} = V_{plume(0)}$. This trend reflects the fact that increasing density from facility pressure reduces the resistance in the plume. We also note that although the ratio of background density from the thruster and facility to the cathode orifice density is assumed to be low, $n_{e(c)}/n_{e(0)} \ll 1$, the contribution of this background density to the overall resistivity of the plume is amplified by the geometric factor L/r. This is reflected by the scaling of the coefficients c_1 and c_2 with $(L/r)^2$ and physically results in the ability of small changes in background gas to have a pronounced impact on the resistive term.

2.5. Simplified model for cathode coupling voltage

Equations (3), (5), and (10) combined yield a model for the cathode coupling voltage as a function of facility pressure. The resulting expression, however, is complex with seven free model parameters, T_e, V_{int}, $V_{b(0)}$, $V_{plume(0)}$, $\bar{P}_T$, c_1, c_2, that represent physical quantities that we do not know *a priori*. While in principle these parameters could be inferred by fitting the model to datasets of coupling voltage as a function of pressure, the parameter space is too large to determine the values with accuracy given the limited size of datasets available (typically 5–10 data points). With this in mind, we make the additional simplifying assumption $c_1, c_2 \ll 1$ (see appendix A). In this limit, we can expand equation (10) around the small quantity $c_1 + c_2 \bar{P}_B \ll 1$ and combine with equation (5) to write equation (3) in the final form

$$V_{cc} = V_{vac} + T_e \ln\left[1 + \frac{\bar{P}_B}{\bar{P}_T}\right] - \left[\frac{T_e}{\bar{P}_T + \bar{P}^*}\right]\bar{P}_B, \quad (12)$$

where we have introduced two additional model parameters, V_{vac} and $\bar{P}^*$. The first, V_{vac}, represents the cathode coupling voltage in the absence of neutral gas originating from the facility ($\bar{P}_B \to 0$). It thus corresponds to the predicted voltage on orbit. The term $\bar{P}^*$ corresponds to the facility pressure where there is a turning point in the coupling voltage. The existence of this maximum is the result of the balance between the Boltzmann contribution (second term in equation (12)) and the resistive contribution (third term) that have opposite trends with facility pressure. These counteracting trends can result in a coupling voltage that is non-monotonic with facility pressure, exhibiting a maximum at $\bar{P}^*$. Expressing equation (12) in terms of this maximum pressure allows us to leverage observed trends in experimental data to restrict the range of possible values for this parameter. We elaborate on this point in the following section.

As a final simplifying step, we make the assumption that $T_e = 5$ eV. This choice eliminates another free parameter in equation (12) and is consistent with the typical range of values reported in previous experimental and numerical studies of hollow cathodes intended for electric propulsion [31, 34, 38, 42]. With this last substitution, we now have

reduced the number of free model parameters in equation (12) to three.

In summary, we have presented in this section a model, equation (12), that is grounded in a first principles analysis of the cathode plume. This result thus provides a physics-based, functional form that can be calibrated against data and applied to make extrapolations to space-like conditions. With this in mind, we turn in the next section to discussing rigorous methods for determining the model parameters and performing the extrapolation.

3. Bayesian parameter estimation

We adopt a probabilistic analysis based on Bayesian statistics to infer the model parameters of equation (12). The advantage of this method is that it rigorously quantifies the uncertainty in the model parameters as well as the credibility in the extrapolation of the model to space-like conditions ($\bar{P}_B = 0$). Following the standard formulation of Bayesian inference, we express the model parameters in vector form as $\Theta = (V_{vac}, \bar{P}_T, \bar{P}^*)$ and the set of measurements (cathode coupling voltage as a function of pressure) as $d = \{(\bar{P}_B^{(1)}, V_{cc}^{(1)}), (\bar{P}_B^{(2)}, V_{cc}^{(2)}), ..\}$. The model parameters are treated as random variables, and the goal is to determine the posterior probability distribution, $P(\Theta|d)$, of these model parameters given the measured data. The expression for this probability distribution stems from Bayes theorem:

$$P(\Theta|d) = \frac{P(d|\Theta) \cdot P(\Theta)}{P(d)}, \quad (13)$$

where $P(d)$ is the Bayesian evidence, $P(\Theta) = P(V_{vac})P(\bar{P}_T)P(\bar{P}^*)$ is the prior probability distribution of the model parameters (assumed to be independent), and $P(d|\Theta)$ is the likelihood.

The prior probability reflects previous knowledge about the distribution of the model fit coefficients. We assume in this work that all the priors are uniform over a prescribed range. For V_{vac}, we use 0–60 V as none of the thrusters we examine exhibited cathode coupling voltages exceeding this range. For the prior distribution of $\bar{P}^*$, we inspect the dataset for the location of the turning point to inform the appropriate range. For example, for datasets that show an evident maximum, we set the prior for $\bar{P}^*$ to be centered on this value with a range of $\pm 20\%$. For datasets that show a monotonically increasing trend in cathode coupling voltage with pressure, we place a lower bound on the prior equal to the maximum pressure at which the data was collected. This reflects the prior belief that, per our model, the maximum occurs at pressures beyond the measured domain. For datasets that show a monotonically decreasing trend with facility pressure, we set the upperbound for the prior distribution as the lowest pressure point that was measured. This encodes the belief that the turning point lies to the left of the dataset—or possibly that there is no turning point for positive pressures. The lower bound on the prior for $\bar{P}^*$ extends to negative values in this latter case. For the prior distribution of $\bar{P}_T$, we recall from the previous section that this parameter represents the ratio of the plasma density from

the thruster to the plasma density originating from the facility at the reference pressure. Depending on the thruster configuration and choice of reference pressure, this coefficient may have a wide range of possible values. We encode this believe by adopting a typical range of 0–50. In order to avoid nonphysical results, we set the lower bound on the range of $\bar{P}_\mathrm{T}$ to ensure that $\bar{P}_\mathrm{T} + \bar{P}^* > 0$.

If we assume that the model with fit parameters Θ is correct, the likelihood function in equation (13) indicates the probability that measurements would yield the dataset, d [48]. To this end, we have chosen an unbiased Gaussian likelihood:

$$P(d|\Theta) = \prod_{j=1}^{N} \frac{1}{\sigma\sqrt{2\pi}} \cdot \exp\left[-\frac{1}{2}\left(\frac{V_\mathrm{cc}^j - V_\mathrm{cc}(\bar{P}_\mathrm{B}^j, \Theta)}{\sigma}\right)^2\right],$$
(14)

where $(\bar{P}_\mathrm{B}^j, V_\mathrm{cc}^j)$ denotes the jth element of the experimentally measured dataset, d; N is the number of points in the dataset; $V_\mathrm{cc}(\bar{P}_\mathrm{B}^j, \Theta)$ is the model from equation (12) with argument $\bar{P}_\mathrm{B}^j$ for the pressure and model coefficients, Θ; and the parameter σ is the standard error in the experimental measurement. The choice of Gaussian likelihood reflects our assumption that experimental measurements of the cathode coupling voltage are normally distributed around the true value.

In this work, we used a nested Markov chain Monte Carlo (MCMC) technique [49] with 10 000 live points iterated 200 000 times to yield a dataset of sampled Θ from equation (13). From this set of parameter values, we generated posteriors for each model parameter by marginalizing the sample distribution. From these marginals, we in turn report the median value of each model parameter and its uncertainty to 95% credibility. To assess the role of the model parameter uncertainty in the fit to data, we evaluated equation (12) for all values of Θ to yield a set of predicted values of V_cc as a function of $\bar{P}_\mathrm{B}$. We plot the median of the model predictions as well as credible intervals that contain 95% of the generated values.

4. Overview of datasets and thrusters

In order to evaluate the proposed model for cathode coupling, we have identified datasets from several previous experimental studies where this voltage was measured as a function of facility pressure (appendix B). In each case, the values for cathode coupling are based on measurements of the plasma potential performed close to the thruster centerline in the far-field and referenced electrically with respect to the cathode. The potential at this location is particularly relevant for assessing the impact on coupling voltage on performance as it best captures the loss to the beam acceleration voltage (figure 2). Before proceeding, we note that we do not consider results from studies that only report cathode to ground voltage as a function of pressure [17, 25, 50, 51].[1] While this is commonly used as a qualitative indication of the cathode coupling voltage, it is not a quantitative measure. This is because there are factors beyond the coupling voltage that can impact the cathode to ground measurement such as sheath potentials and the facility's electrical configuration. With this in mind, in this

section we overview the thrusters we examined, each dataset that we used, and how we extracted the data.

4.1. SPT-100

The SPT-100 is a 1.35 kW Hall thruster developed by the Fakel Experimental and Design Bureau that operates at a discharge voltage of 300 V and with the cathode mounted external to the main discharge. The dataset we use for analysis is from reference [15] in which far-field radial sweeps at a distance of 1 m were performed to measure the plasma potential with respect to facility ground as a function of facility pressure. We have converted these data to cathode coupling voltage by subtracting measurements of the cathode to ground voltage that also were made during this campaign[1]. The uncertainty on the reported data was estimated as 2 V. Reference [15] reports the same set of measurements for two different facilities, the L3 chamber and the Aerospace corporation chamber. We consider both datasets in this work.

4.2. PPS 1350-G

The PPS 1350-G is a 1.35 kW Hall thruster from Snecma that operates at a discharge voltage of 300 V with a cathode mounted external to the main discharge. We use for our analysis the dataset of coupling voltage versus facility pressure as reported in reference [52]. These measurements were collected in the same way and in the same locations as for the SPT-100, but the authors directly report the plasma potential with respect to cathode potential. There thus is no need to correct for the cathode to ground potential. The uncertainty on the reported data was 2 V.

4.3. BHT-1500

The BHT-1500 is a 2 kW class Hall thruster developed by the Busek Corporation that can operate with a cathode either in an internal, center-mounted position or in a location external to the discharge. Reference [53] reports measurements of the BHT-1500's response to variations in facility pressure for both cathode configurations at the operating condition of 300 V and 1.8 kW. In this work, radial sweeps were performed with a Langmuir probe in the thruster far-field at a distance of 1 m. These measurements were used to infer plasma potential as measured with respect to the cathode with an uncertainty of 0.2 V.

4.4. H9

The H9 is a 9 kW class magnetically-shielded thruster that was jointly developed by the University of Michigan, the Jet Propulsion Laboratory, and the Air Force Research Laboratory. The thruster employs a center-mounted, internal cathode in its default configuration. We use in our analysis the dataset from reference [54] where a Langmuir probe was employed to measure the H9's plasma potential referenced with respect to

---

[1] The cathode to ground voltage was measured for the experiment described in reference [15] but not reported. K Diamant has provided these measurements through personal correspondence.

the cathode as a function of facility pressure. The measurement location was on thruster channel centerline, 40 cm downstream of the exit plane. The measurement error was reported with values ranging from 0.5 and 2 V.

4.5. HERMeS

The Hall effect rocket with magnetic shielding (HERMeS) is a 12.5 kW class thruster with an internally mounted cathode developed by the Jet Propulsion Laboratory and the NASA Glenn Research Center. We use in our analysis data from reference [20] in which a Langmuir probe was employed to make local measurements of the plasma potential with respect to ground in the far field. As with the dataset from the SPT-100, we converted these reported values to cathode coupling voltage by subtracting the cathode to ground voltage.[2] The reported uncertainty in these measurements was ± 4 V. Several voltages and operating conditions were considered in this previous study, though we only examine representative results for a low voltage, low power condition (300 V and 4.5 kW) and a high voltage, high power condition (500 V and 12.5 kW).

4.6. HiHVAc

The high-voltage Hall accelerator (HiVHAc) is a 3.9 kW class Hall thruster designed by the NASA Glenn Research Center that employs an externally-mounted cathode. Reference [18] reports measurements of this thruster's plasma potential with respect to cathode as a function of pressure at a location 10 cm downstream of the thruster exit. We use for our analysis the results from two operating conditions investigated in this study, 300 and 500 V at 3 kW. As the error in these measurements was not reported in reference [18], we assign an uncertainty based on the nearest significant figure of the data, ± 1 V.

4.7. NASA-173M

The NASA-173M is a 5 kW class laboratory Hall thruster designed by the NASA Glenn Research Center and the University of Michigan. Its cathode is located external to the main discharge. We use for our analysis the results from reference [55] in which a Langmuir probe was swept at a 1 m radius to measure the plasma potential in the thruster far field with respect to the cathode at the 4.5 kW and 300 V condition. The measurement uncertainty is reported as ± 0.2 V. Reference [55] includes datasets for the cathode in its nominal position ($Y = 0$) with respect to the thruster and moved laterally $6''$ away from the thruster centerline ($Y = 6$). We consider both datasets in our analysis.

5. Results

We present in the following the results of applying the model for cathode coupling voltage to experimental data. We first

show examples of the posterior distributions resulting from Bayesian parameter estimation. We then compare model fits directly to each dataset described in the preceding section, reporting the corresponding model parameters and our confidence in these parameters. For each dataset, we use the reference pressure $P_{\text{ref}} = 10^{-5}$ Torr-xenon. This value is the historical standard proposed by Randolph [2] for the maximum allowable facility pressure in order for thruster performance measurements to be indicative of on-orbit behavior.

5.1. Sampled posterior distribution

Figure 3 shows the posterior distributions generated for the model parameters of equation (12) when applied to the SPT-100 (L3) dataset with a reference pressure of $P_{\text{ref}} = 10^{-5}$ Torr-xenon. The figure includes the one-dimensional marginal distributions $(P(V_{\text{vac}}|d), P(\bar{P}_{\text{T}}|d), P(\bar{P}^*|d))$ as well as the two-dimensional joint distributions, $(P(V_{\text{vac}}, \bar{P}_{\text{T}}|d), P(V_{\text{vac}}, \bar{P}^*|d), P(\bar{P}_{\text{T}}, \bar{P}^*|d))$. The marginal distributions are normalized to unity while the contours in the joint distributions represent the total percentage of samples that are contained below the contour. We note that figure 3 is a representative example, exhibiting the same qualitative features as found in the other cases.

The shapes of these distributions for each model parameter can be interpreted through the definitions introduced in the previous section. For example, the most probable value of $V_{\text{vac}} = 31.1$ V, which corresponds to the peak in this distribution, is the most probable prediction for the cathode coupling voltage under space-like conditions. The relatively narrow width of the distribution compared to the most probable value suggests a high confidence in this prediction. The most probable value of $\bar{P}_{\text{T}} = 1.5$ indicates that at the connection point, P, the plasma density from the thruster is approximately 150% of the plasma originating from the facility at the reference background pressure. The comparatively larger width of the distribution relative to the magnitude of the most probable value indicates less confidence in this estimate, though the distribution still exhibits a well-defined peak. The median value of $\bar{P}^* \approx 2.6$ indicates the normalized pressure that corresponds to the maximum cathode coupling voltage, i.e. where the resistive effects start to overcome the Boltzmann contribution.

The joint distribution functions in figure 3 represent graphically the correlations between the model parameters. The fact that the contours generally follow non zero slopes suggests that the parameters may be physically linked. This result is not unexpected given that all the coefficients are related to local plasma properties that stem from the same sources, the thruster and cathode. With that said, while further exploring the physical underpinnings of these correlations is beyond the scope of this investigation, we note the fact that these parameters are correlated means the posteriors cannot be treated as statistically independent.

5.2. Model comparison to data

We show in figure 4 the model fits compared to the data for each configuration discussed in section 4. As described in section 3, we generated these plots by employing an MCMC
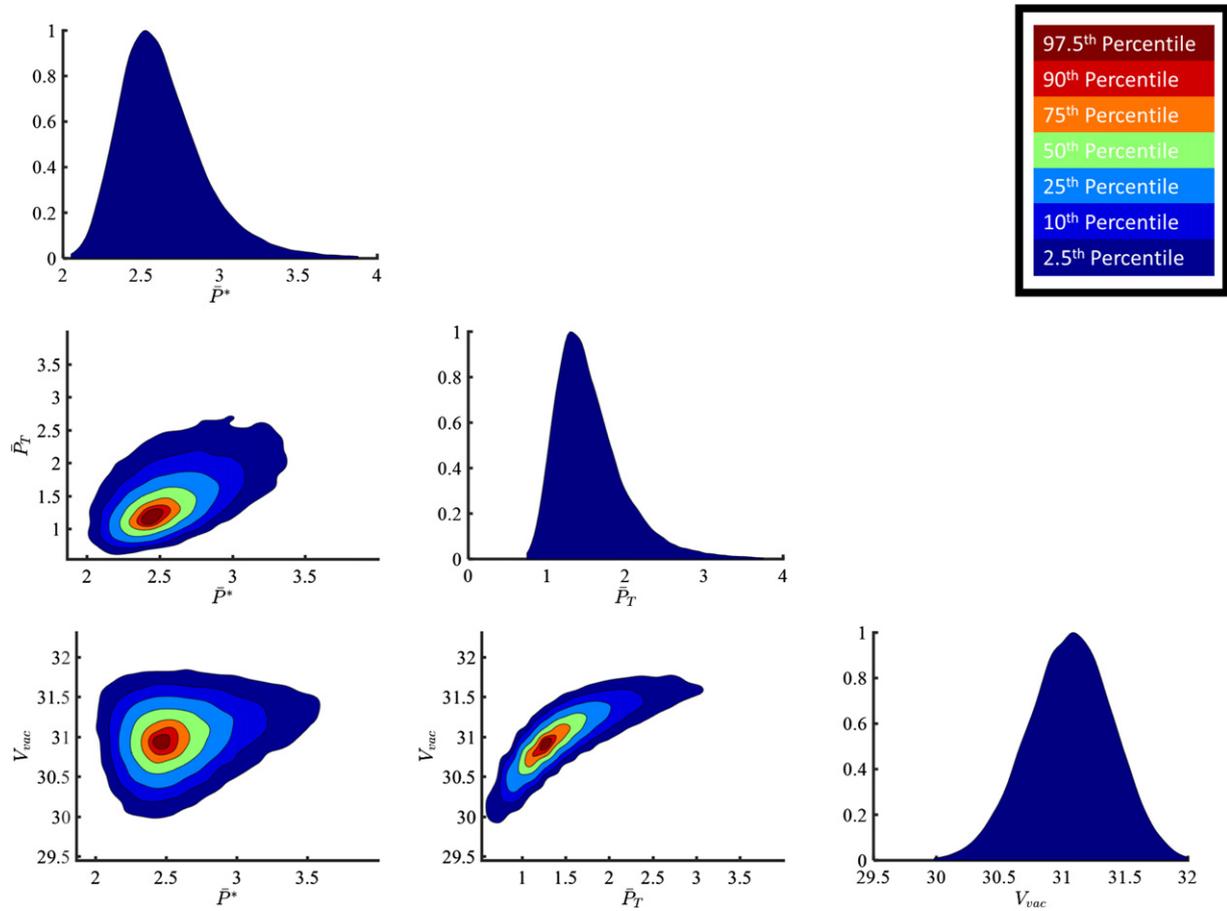
---

[2] The potential and cathode to ground voltage were measured for the study in reference [20] but not reported. W Huang has provided these measurements through personal correspondence.

Figure 3. Posterior distributions of the model parameters for the SPT-100. This dataset corresponds to the test performed in the L3 facility. Results are based on 10 000 samples. The reference pressure is $P_{\mathrm{ref}} = 10^{-5}$ Torr-xenon.

algorithm to sample from the posterior of each distribution 10 000 times. At each pressure, we then calculated the median (black line) and 95% credible interval (dashed lines) from the samples. These trends are superimposed on the experimental data. We also have extrapolated the curves to zero normalized pressure, $\bar{P}_B = 0$, to illustrate the model predictions and confidence for on-orbit behavior. The expansion of the credible intervals at this extrapolated point in each case reflects the fact that in the absence of data in this region, our confidence in the model decreases. The magnitude of the spread in the intervals is a direct function of the uncertainty in the reported data.

Although the coupling voltage in each case is less than 40 V, the trends of the cathode voltage with facility pressure vary substantially. This precludes us from making a broad generalization about how coupling voltage responds in all thrusters, i.e. we cannot uniformly state coupling voltage improves or worsens with pressure. However, we do find our proposed model is able to fit the indicated trends in all cases. This speaks not only to the versatility of the scaling law but provides qualitative validation of our governing hypothesis that there are two disparate effects—the Boltzmann and resistive terms—that drive the coupling. The fact that there are different trends in coupling voltage with pressure suggests that each thruster environment facilitates a different balance between these two processes.

To this point, figures 4(a)–(c) show the results for the PPS 1350-G, H9, and BHT-1500 with internal cathode where in each case, the cathode coupling voltage increases with facility pressure. In the context of the proposed model, this suggests that the Boltzmann contribution to the coupling voltage is dominant. On the other hand, figures 4(d)–(h) show the datastets for the BHT-1500 external cathode configuration, the NASA-173M, and the HiHVAc thruster. In each case, the coupling voltage decreases with facility pressure. This indicates that the resistive contribution to the coupling voltage drives the coupling response. We note here as well that the credible intervals for the NASA-173M are narrower than any other dataset and in some cases do not enclose the data. This stems directly from the fact that the reported uncertainty on these measurements was the lowest of all the datasets. Figures 4(i) and (j) show measurements and model fits for the HERMeS thruster with its center mounted cathode. In a departure from the other results, these plots exhibit a coupling voltage that is nearly constant with changing facility pressure. This might indicate that there is higher confidence that the ground test results are more representative of an in-space environment, though this conclusion is tempered by the fact that the uncertainty in this data is higher compared to the other results. Finally, figures 4(k) and (l) show the datasets and model fits for the SPT-100 from measurements performed in the L3 and Aerospace
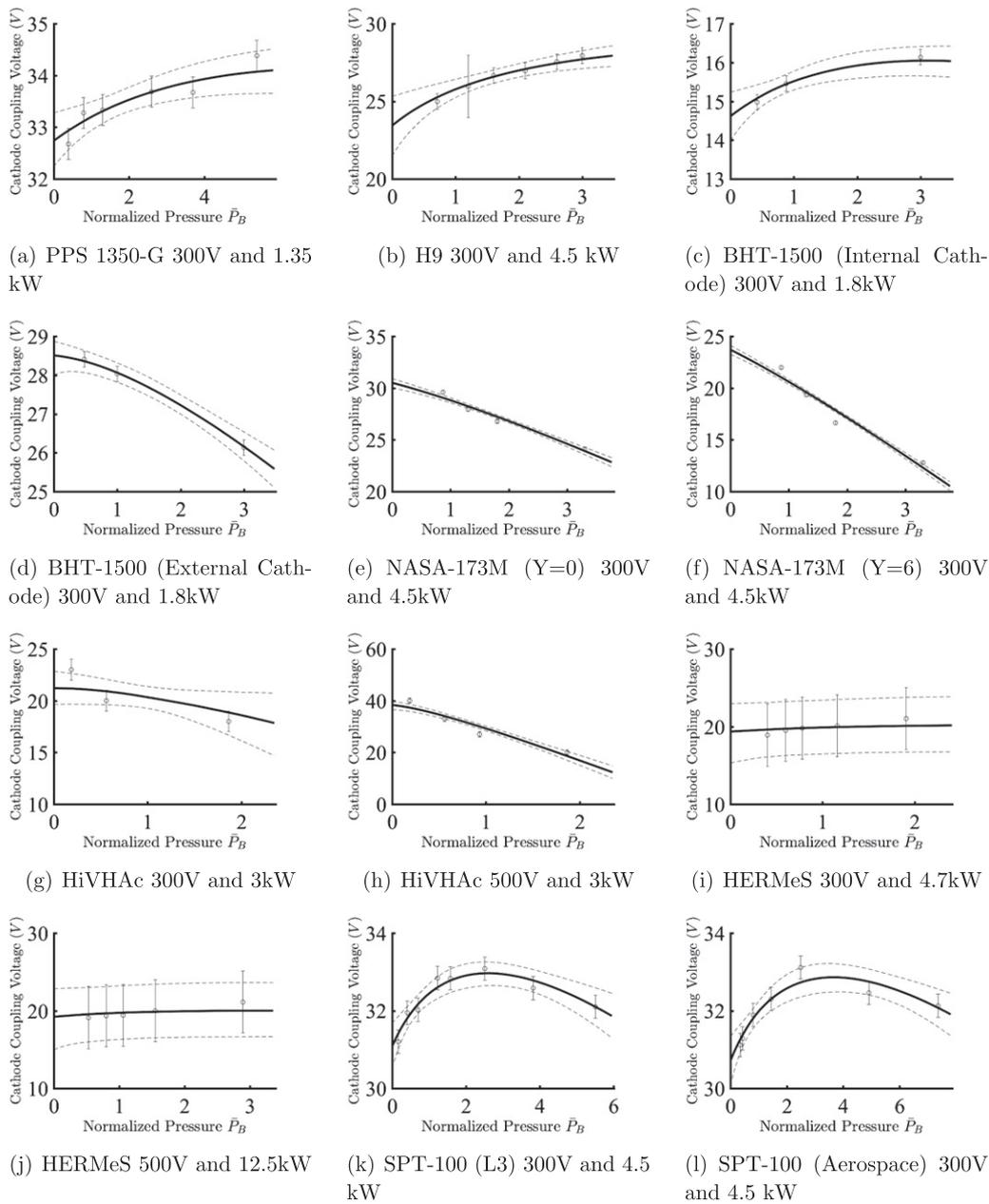
Figure 4. Median model fits (black solid line) bounded by 95% credible intervals (dashed lines) for 12 thruster configurations. All pressures have been normalized to the same reference, $P_{ref} = 10^{-5}$ Torr-xenon.

Corporation facilities. Unlike the trends for the other thrusters, the SPT-100 data shows an evident turning point at $\bar{P}_B = 2 - 3.5$. This is consistent with the marginal distributions presented in figure 3. In keeping with the physical underpinnings of our model, this trend indicates that in the SPT-100 there is a transition from when the Boltzmann contribution dominates at lower pressures to the resistive term driving the coupling voltage at higher pressures.

Beyond the evident trends with pressure, figure 4 also affords qualitative insight into the role of cathode placement and facility. For example, the results from the BHT-1500 illustrate the fact that cathode placement in the same thruster can lead to a fundamentally different response to the facility environment (figures 4(c) versus (d)). Our model is able to

capture this transition, once properly calibrated against the data. Similarly, figures 4(e) versus (f) for the NASA-173M illustrate the impact of translating the cathode away from the thruster. Although the trend with pressure remains the same, the cathode that is farther from the discharge ($Y = 6$) exhibits a more sensitive dependence on pressure, decreasing by a factor of 50%. This is contrasted with the 17% reduction exhibited by the cathode located at $Y = 0$. Finally, the SPT-100 datasets, which were taken at two different facilities, exhibit quantitative agreement in magnitude and trends. This suggests that differences in the test facilities appear to have little impact on the sensitivity of this parameter to facility pressure. We discuss this result as well as the other trends in more detail in section 6.

Table 1. Median and the 2.5th and 97.5th percentiles of the marginal posterior distributions for the model parameters for each dataset. The same reference pressure of $\bar{P}_{\text{ref}} = 10^{-5}$ Torr-xenon was used in each case. V_D denotes discharge voltage and P_D is discharge power in kilowatts.

Thruster/cathode	V_D/P_D	$\bar{P}^*$			$\bar{P}_T$			V_{vac}		
		$P_{2.5}$	P_{50}	$P_{97.5}$	$P_{2.5}$	P_{50}	$P_{97.5}$	$P_{2.5}$	P_{50}	$P_{97.5}$
PPS 1350-G/Ext.	300/1.35	4.6	7.8	9.9	3.2	5.6	11.5	32.2	32.7	33.3
H9/Int.	300/4.5	4.0	7.4	9.8	0.6	1.3	2.9	21.5	23.5	25.3
BHT-1500/Int.	300/1.8	2.3	3.2	3.9	1.3	2.3	5.0	14.0	14.6	15.2
BHT-1500/Ext.	300/1.8	−0.9	−0.3	0.6	1.4	2.8	3.8	28.0	28.5	28.9
NASA-173M ($Y=0$)/Ext.	300/4.5	−2.0	−1.5	−0.7	2.2	3.2	3.7	30.0	30.5	30.9
NASA-173M/Ext. ($Y=6$)/Ext.	300/4.5	−2.0	−1.8	−1.2	2.2	2.8	3.1	23.3	23.7	24.1
HiVHAc/Ext.	300/3	−0.5	−0.1	0.7	0.7	1.6	8.6	19.6	21.2	22.8
HiVHAc/Ext.	500/3	−0.2	−0.1	0.0	0.3	0.5	0.5	36.5	38.3	39.8
HERMeS/Int.	300/4.7	1.6	3.3	4.9	0.7	5.2	9.7	15.3	19.4	22.9
HERMeS/Int.	500/12.5	1.6	3.3	4.9	0.6	5.3	9.7	15.0	19.2	22.8
SPT-100 (L3)/Ext.	300/1.35	2.2	2.6	3.3	1.0	1.5	2.7	30.5	31.1	31.7
SPT-100 (Aerospace)/Ext.	300/1.35	3.2	3.7	4.6	1.2	1.8	3.3	30.1	30.7	31.3

5.3. Model parameters and predictions for on-orbit conditions

We summarize in table 1 the statistical properties of the model fits shown in figure 4. Here we list the operating condition, the median value of the model parameter, and the bounds, denoted $P_{2.5}$ and $P_{97.5}$, that contain the most probable 95% of the samples. We employed these latter metrics to represent the relative skewness of the distributions.

From this table, we see the median value of $\bar{P}_T$ varies between 0.5 and 5.6. In light of the definition of this parameter, this result suggests that in all of these devices, the plasma density originating from the thruster is within an order of magnitude of the plasma density that comes from the facility at the reference pressure. This result is not unexpected given the provenance of the reference pressure, P_{ref}, which was chosen by Randolph *et al* [2] to represent a threshold density where the flux of neutrals into the thruster from the facility becomes commensurate with the flux of neutrals originating from the thruster. For most of these reported values, the variance in the parameter (as represented by the credible intervals) is smaller than the median.

The trends in $\bar{P}^*$ mirror the trends in coupling voltage with pressure shown in figure 4. Smaller values of $\bar{P}^*$ denote conditions where the data decreases with facility pressure and resistive effects dominate. Higher values of $\bar{P}^*$ correspond to the opposite trend where Boltzmann effects govern the coupling voltage. The cases with intermediate values of this model parameter (SPT-100) indicate the existence of turning points in the data.

The vacuum voltages, V_{vac}, in table 1 represent the expected coupling voltage at zero facility pressure, i.e. a space-like environment. In general, the confidence in these predictions, as represented by the variance compared to the median value, is high. The projected values similarly have a relatively narrow range, 15–40 V. Notably, the thrusters with internal cathodes appear generally to exhibit lower vacuum coupling voltages than the thrusters with externally-mounted cathodes. Physically, this suggests that these thrusters have a better

electrical connection to the main thruster discharge. We return to this point in section 6

We conclude this section by remarking on the practical significance of these results. We have demonstrated the ability to use a physics-based model combined with data to not only generate predictions for coupling voltage on orbit but to quantify our confidence in these predictions. This has practical implications for thruster testing programs. Provided operators can generate the types of parametric datasets shown in figure 4 for their thrusters, our approach offers the capability to make physics-based, rigorous assessments of on-orbit behavior for this particular aspect of thruster operation.

6. Discussion

We have shown in the previous section the efficacy of our simplified model to describe experimental data for cathode coupling voltage as a function of pressure. We similarly have rigorously quantified the uncertainty in the model parameters and in turn how this impacts predictions for zero background pressure. We expand upon these results here by examining the validity of the underlying assumptions of the model, the physical significance of the trends in the model parameters, how our result compares to previous work, and the application of our model for predicting thruster performance on-orbit and for identifying strategies to mitigate this facility effect.

6.1. Implications of relaxing the model assumptions

There were a number of assumptions we invoked in the derivation of equation (12). The most critical include constant electron temperature, the simplified model for the expansion of the plume, and the neglect of cross-field transport. We discuss in the following the implications of relaxing each of these assumptions.

6.1.1. Constant electron temperature. The assumption that the electron temperature is constant with facility pressure is not strictly self-consistent with the model we have presented. In particular, we argued in section 2.4 that with decreasing

facility pressure, the electron resistivity will increase. This stems from the form of the anomalous collision frequency we invoked from reference [42]. While this increase in resistivity will result in a higher contribution to the coupling voltage from the resistive component, it also will lead to increased Ohmic heating in the near-field cathode plume. The electron temperature therefore may increase at lower facility pressure.

Estimating the change in electron temperature self-consistently and how it impacts the model for coupling voltage would in principle require an equation for the electron energy. The addition of such an equation would destroy the simplicity of the algebraic functional form we have derived in this approach. Bearing this in mind, we can point to indirect evidence that the variation in near-field electron temperature may be a weak effect. Numerical simulations and experimental measurements have shown over a wide range of thruster and facility configurations that electron temperatures range from $T_e = 2$–6 eV. This relatively narrow range suggests indirectly that this quantity may not depend strongly on the facility environment. As an additional consideration, we note that although the temperature's dependence on pressure is not known *a priori*, in the limit that it is a weak dependence, it can be approximated to first order with a linear term, i.e. $\Delta T_e \propto -\Delta \bar{P}_B$. The temperature dependence thus in part can be captured by the linear relationship already exhibited in equation (12).

6.1.2. Cathode plume expansion model. Another key assumption we have employed in our analysis is that the plume expands conically from the cathode exit (equation (9)). While this simplification has been invoked in previous 1D models and validated against measurements of plasma properties along cathode centerline [44], there is a possible ambiguity in this simplification that stems from θ, the assumed angle of expansion. This model parameter depends on the cathode operating condition, and in principle, it will impact the form of the resistive term in equation (12). In our approach, we have eliminated this model parameter implicitly by expanding equation (9) under the dual assumptions that $r/L \ll 1$ and that the plasma density from the thruster in the cathode plume and the facility background are both small compared to the density in the cathode exit.

These assumptions could be relaxed by using the full form of equation (9) in equation (6) when evaluating the integral. However, this will have the consequence of introducing an additional model parameter, θ, which must be inferred against data. As we discussed in section 2.5, the limited size of available datasets has driven us to eliminate as many model parameters as possible. With that said, given that we anticipate both of the assumptions we have invoked to remove θ will be universal across thruster types, the neglect of this free parameter can be employed without a loss in model fidelity.

6.1.3. Cross-field transport. We have assumed in the preceding discussion that the electron dynamics in the cathode near field are parallel to the applied magnetic field. This is justified provided the electrons remain sufficiently magnetized that the path of least resistance is along the field lines. In practice,

for cathodes placed farther from the thruster body where the magnetic field is lower, it may be possible for finite current to cross field lines, thus changing the form of equation (6). With that said, even in this limiting case, we anticipate that the form of equation (12) will still capture the correct behavior.

To illustrate this, we re-examine equation (2) for the case when crossed-field transport is permitted. As this equation shows, the resistivity in the cross-field direction depends inversely on the collision frequency in the $\hat{\parallel} \times \hat{\perp}$ direction. As was found in reference [42], however, the collision frequency in this direction scales linearly with neutral density. We therefore anticipate that qualitatively, even allowing for cross-field transport, the resistivity in the near-field will vary inversely with facility pressure. Thus, while including cross-field effects may ultimately lead to a more complex dependence of the resistive term in equation (12) on facility pressure, at least qualitatively, the trend of decreasing resistance with facility pressure is still anticipated and represented by our simplified model.

The preceding argument applies to the case where the magnetic field is sufficiently weak that electrons emerging from the cathode immediately can cross field lines. However, we note that in some thrusters with external cathodes, the cathode is located in a region of strong magnetic field that is outside the so-called thruster 'separatrix.' The BHT-1500 in the external configuration, for example, conforms to this design [53]. In this case, the electrons are confined to field lines, but there are no lines that directly connect the cathode plume to the thruster. This would suggest that for the current path to be completed, there must be a point downstream of the cathode plume where cross-field transport, i.e. across the separatrix, does occur.

The necessity of this cross-field transport does not invalidate the model we have proposed here. Indeed, although we have illustrated in figure 1 a case where there is a well-defined field line that connects to the main plume, in practice we only assume in our model that the electron dynamics in the *near-field* region of the cathode must be parallel to the field lines. The resistive term only captures the effect of the resistivity of the electrons as they initially follow the applied field. Downstream of this region, i.e. characteristic length L, we assume that the anomalous resistivity is negligible and the plume dynamics are strictly Boltzmann. Implicit in this assumption is that electrons have sufficient mobility along and across field lines to maintain a Boltzmann relationship between density and potential in the far-field region. If this indeed the case for a cathode located outside the separatrix, the model still applies.

To this point, qualitatively, the results in reference [53] for the cathode located outside the separatrix show that the electron plume appears to follow field lines by moving away from the thruster. This would be the region where resistive effects occur per our model. Presumably, connection to the main plume occurs further downstream where the plasma may be more Boltzmann. The ability of equation (12) to capture the pressure dependence of the coupling voltage for this case (figure 4d) is a correlational indication of its validity.

6.2. The need for anomalous collision frequency to explain observed trends

We discuss here how anomalous collision frequency is necessary in order for the resistive term in equation (12) to show improved coupling (lower voltage) with facility pressure. To illustrate this, we consider the parallel component of resistivity in equation (2) in the limit where only classical collisions dominate:

$$\eta_\parallel = \frac{m_e}{q^2 n_e} \left[\nu_{ei} + \nu_{en} \right], \tag{15}$$

where ν_{ei} is the electron–ion collision frequency and ν_{en} is the electron–neutral frequency given by (cf reference [44])

$$\nu_{ei} = 2.9 \times 10^{-12} n_e \frac{\ln \Lambda}{T_e^{3/2}}$$

$$\nu_{en} = 6.6 \times 10^{-19} \left[\frac{\frac{T_e}{4} - 0.1}{1 + \left(\frac{T_e}{4}\right)^{1.6}} \right] n_n \sqrt{\frac{8 T_e}{\pi m_e}}. \tag{16}$$

Here Λ denotes the Coulomb logarithm, n_n is the local neutral density, and T_e is given units of energy. Assuming that the background neutral density will scale with the local electron density and that the temperatures remains approximately constant, we see that in the limit of classical collisions, $\eta_\parallel$ will be constant. This would suggest that resistive contribution to the cathode coupling voltage would be independent of facility pressure, which is not reflected by the data (figures 4(d)–(h)). Rather, it is the unique form of the anomalous collision frequency and its dependence on density that has yielded a model that captures the experimentally observed trends.

6.3. Impact of cathode placement and facility configuration on trends in coupling voltage

Interpreted in the context of our model, three of the datasets shown in figure 4 can provide insight into the impact of cathode environment on the response to facility pressure. The first set consists of the plots from the BHT-1500 (figures 4(c) and (d)). In this case, the thruster was operated at the same operating condition but with the cathode located at two locations, internally mounted and externally mounted. Evidently, the different locations yield disparate trends in facility pressure. In the context of our model, the internal cathode appears to be dominated by Boltzmann effects (coupling voltage increases with facility pressure) while the external cathode configuration's response is driven by resistive effects (coupling voltage decreases with pressure).

This disparity in trends may be attributed to local changes in the cathode environment between the two configurations. For example, since the external cathode is located outside the magnetic field separatrix for the BHT-1500, the electrons must follow a more divergent path to reach the discharge. This may contribute to a longer effective electrical path and therefore resistance. To this point, looking to the results reported in table 1, we see that the internal cathode is projected to have a vacuum voltage that is 14 V lower than the external configuration. Qualitatively, this suggests that the external cathode has a more tenuous electrical connection to the main discharge. A

similar difference between external and internal cathodes was noted in the parametric study Hofer and Anderson performed on a 6 kW class device [17].

Figures 4(e) and (f) show the results for the NASA 173M at the same operating condition but with the cathode at two different radial locations. In both configurations, we see that the coupling voltage trends down with facility pressure. This suggests in light of our proposed model that resistive effects dominate. With that said, there are two salient differences: the cathode closer to the thruster has a higher vacuum coupling voltage (~ 30 V versus 24 V), but the cathode farther from the thruster exhibits a more drastic change in voltage with pressure. These results indicate that the more radially distant cathode is positioned to better couple electrically couple to the main discharge; however, its position renders it more susceptible to facility changes. One potential explanation for this discrepancy is that the more radially distant cathode may intercept fewer particles originating from the main discharge. The baseline density in the cathode plume therefore will be lower. This translates to a smaller value of $\bar{P}_T$ and therefore a steeper slope for the dependence of coupling voltage on pressure. This hypothesis is supported by the median values of the coefficients shown in table 1.

Figures 4(k) and (l) show the cathode coupling voltage for the SPT-100 at the same operating condition but in two different facilities. The quantitative agreement between the results suggests that the cathode coupling response to facility pressure, at least for this thruster, is not a function of the facility boundary conditions (e.g. the electrical coupling to the walls). Rather, it is a localized effect. This is consistent with the physical interpretation underlying our model. We have stipulated that it is the local resistivity in the cathode plume and local disparity between the cathode plume density and the plasma density originating from the thruster that drive the coupling's response to the facility environment.

6.4. Comparison to previous cathode coupling models

The analytical model we have presented in the preceding discussion is based on a number of key assumptions consistent with experimental measurements of cathode and Hall thruster plasmas. With that said, there have been at least three previous attempts to derive simplified models for the dependence of cathode coupling voltage on pressure [19, 31, 33]. In each case, the underlying assumptions of the models differed from the ones we have proposed here, and yet, they were able to recreate experimental trends. This begs the question as to which model, if any, correctly represents the physical processes in the plasma. With this in mind, we briefly discuss the previous models, their underlying assumptions, and how these compare with our physical interpretation.

6.4.1. Spektor model.
Spektor *et al* [19] employed a 1D numerical model to determine the cathode coupling voltage of the SPT-100 as a function of facility pressure. Their approach differed from ours in that they assumed the electron collisions were classical and that the current path could cross the applied field. Per our discussion in section 6.1, this latter assumption is

not consistent with typical cathode plasma conditions. Indeed, the electron resistivity across field lines is orders of magnitude higher than in the parallel direction, which should thus direct the current along the applied field.

As the authors point out in reference [19], they are able to artificially promote cross-field current by lowering the magnetic field strength by an order of magnitude compared to typical conditions. This was necessary as it is the inverse dependence of cross-field mobility on the collision frequency (equation (2)) that allowed the authors to capture the correct trends in coupling voltage with density (the parallel resistivity for classical collisions is independent of facility pressure—section 6.2). The authors note that the choice to lower the magnetic field was driven by expedience and remark that the presence of anomalous collisions could be another possible mechanism for enabling cross-field transport. However, as we have shown in this study, experimentally, the anomalous collision frequency in the cross-field direction is still too low to allow for significant current to flow locally in this direction. With that said, finite current could flow azimuthally if the effective area through which the current couples to the main discharge is assumed to be larger than just the local area subtended by the cathode plume. This effect is not included in the Spektor model, but it is an assumption employed in the approached adopted by Mikellides (section 6.4.3).

6.4.2. Cusson and Jorns model. Cusson and Jorns [33] derived a model for cathode coupling voltage based on the assumption that the electron transport was non-classical and dominated by resistivity driven by IAT. Although our approach is predicated on the same assumption, we differ from this previous work in two ways: this earlier study neglected the Boltzmann contribution and it treated the effect of the IAT differently. Cusson and Jorns assumed the IAT grew as it convected without saturating in the plume. Our model, on the other hand, is based on the assumption that the waves are saturated, thus giving rise to the simple closure expression for collision frequency we have adopted (equation (7)). Ultimately, both models are able to be tuned to match experimental trends in cathode coupling voltage with pressure. However, the fact that our model for the IAT has been validated against a cathode plume, [42] lends additional support to the approach we have presented here.

6.4.3. Mikellides model. The final model for comparison was proposed by Mikellides *et al* [31]. This work was motivated by the need to explain experimental trends for the cathode coupling voltage in the 4.5 kW-class SPT-140 thruster. The derivation of this model was informed by high-fidelity numerical simulations of the SPT-140 that had been benchmarked against experimental data [32]. The final algebraic model presented in reference [35] has the same form as equation (12) with two exceptions: the resistive term is absent and the sign of the Boltzmann term is reversed.

The differences in the models stem from the underlying assumptions about the electron coupling. Instead of restricting the coupling to the localized near-field of the cathode plume, Mikellides *et al* assume electrons from the cathode can flow in both the axial and azimuthal directions. Some electrons sourced from the cathode can cross the magnetic field and then turn axially toward the main discharge. The net effect is that the current from the cathode can be represented as electrons coupling axially to the main discharge along the entire annulus the cathode subtends. Mikellides *et al* assume that the variations in the coupling voltage can be attributed to azimuthal asymmetries in this current that result from changes in facility pressure. As a consequence, even though the authors in reference [31] note that electron coupling to the discharge occurs along field lines and that non-classical electron resistivity along field lines can develop in cathode plumes, they assume that the response of these effects to facility pressure can be neglected compared to the changes that result from pressure-induced variations in the azimuthal distribution of current. This dependence is represented with a Boltzmann-like scaling.

The electron coupling through the entire annulus subtended by the cathode is modeled in the numerical axisymmetric simulations that were used to guide the Mikellides approach by scaling the plasma density at the cathode by the ratio of the area of the cathode exit to the area of the annulus. This scaling conserves the total current from the cathode while reducing the effective density at the radius of the cathode such that the inequality $n_{e(P)}^{T} \gg n_{e(0)}$ is satisfied. This latter assumption explains why the Boltzmann contribution to the plasma potential is positive in the Mikellides model (in contrast to our form where we assume the opposite inequality for the density). It is ultimately because of this sign change that the coupling voltage improves with facility pressure in the Mikellides model. Mikellides *et al* similarly introduce a coefficient α to represent the change in the voltage drop due to azimuthal asymmetry in the axial current density. This functionally allows for an adjustable parameter to better match experimental trends in voltage with facility pressure.

Practically, both our result and the Mikellides model (when properly tuned with fit coefficients) are able to represent experimental trends in the cathode coupling voltage for thrusters with external cathodes. However, the physical reasons for the decrease in coupling voltage with pressure are fundamentally different: our model attributes it to a change in parallel resistivity while the Mikellides approach ascribes the change to a Boltzmann-like effect. While the ambiguity about which description is valid may only be resolved through direct experimental measurements of the electron transport properties, the arguments we have made in our comparison to the Spektor model about the high-resistivity in the cross-field direction favoring local transport of electrons along field lines still pertains. Similarly, we remark that qualitatively, external cathode plumes (as denoted by the region of high luminescence) typically follow the applied field structure (cf long exposure images from reference [53] for the BHT-1500). This lends correlational support to our assumption that the connection to the plume is a localized process. With that said, luminosity in plasma is a qualitative metric at best, and this observation does not discount the possibility the electron dynamics could be connecting to the plume at other azimuthal locations.

As a final comment, we remark that models from reference [31] as well as from [19, 33] all uniformly predict that the cathode coupling voltage should decrease with facility pressure. There are experimental cases, however, where the opposite trend occurs (figures 4(a)–(c)) or there is non-monotonic behavior (figures 4(k) and (l)). The limitation of these previous approaches to capture these trends may be attributed to the fact that the assumptions underpinning these models are only valid for the particular thruster that was studied. Indeed, in each of these previous cases, the data from only one thruster was considered and used to evaluate the model in question. Our approach in principle has expanded versatility as we have included terms that represent two disparate physical processes—the resistive and Boltzmann contributions—that can be varied in magnitude by changing the model coefficients. This allows us to represent different cathode environments where one may effect may dominate over another. We therefore are able to capture with a high degree of confidence the varying trends exhibited by different cathode configurations.

6.5. Implications for thruster performance models

As we have discussed in the introduction, the guiding goal of developing a physics-based model for the coupling voltage is to be able to predict key properties of the thruster on orbit. To this end, we consider here our result in the context of a performance model for the thruster where following reference [44], we can express thrust as a product of scalar terms:

$$T = \cos\theta_{\mathrm{D}} \sqrt{2\eta_{\mathrm{b}}\eta_v\eta_m\eta_0 \dot{m}_{\mathrm{p}} P_{\mathrm{in}}}. \tag{17}$$

Here P_{in} denotes the input power to the thruster, $\dot{m}_{\mathrm{p}}$ is the mass flow rate through the thruster and cathode, θ_{D} is the divergence angle of the plume, η_{b} is the beam current utilization efficiency that indicates the fraction of the supplied discharge current that is converted to accelerated ion current, η_m is the mass utilization efficiency, η_0 is an electrical conversion efficiency from the power supply to the thruster, and η_v is the voltage utilization efficiency which represents the fact that not all of the applied electrostatic potential energy for accelerating the exhaust is converted to ion kinetic energy (figure 2).

For most facility pressure studies, the discharge current—and by extension—power is held constant. The dependence on facility pressure thus stems from the other terms in equation (17), e.g. $\theta_{\mathrm{D}}(\bar{P}_{\mathrm{B}}), \eta_{\mathrm{b}}(\bar{P}_{\mathrm{B}}), \eta_v(\bar{P}_{\mathrm{B}})$, etc. Our effort in this work has informed a physics-based model for one of these efficiencies:

$$\eta_v = 1 - \frac{V_{\mathrm{cc}}(\bar{P}_{\mathrm{B}}) + \Delta V}{V_{\mathrm{D}}}, \tag{18}$$

where $V_{\mathrm{cc}}(\bar{P}_{\mathrm{B}})$ is given by equation (12) and ΔV denotes other contributions to losses in the discharge voltage such as spatially-distributed ionization and sheath formation. In light of the experimental data shown in figure 4 and our model-based extrapolations to space (V_{vac} in table 1), equation (18) would indicate that the change in cathode coupling voltage can lead to 1%–5% variations in thrust from the highest pressure conditions.

Ultimately, to predict the thrust in space, it is necessary to determine physics-based models for the other terms in equation (17), and indeed, there are active efforts exploring these other effects [30, 31]. With that said, it has been suggested [31] that at least for some thrusters such as the SPT-140, the variation in the cathode coupling may be one of the dominant factors impacting thrust.

6.6. Facility effect mitigation

As a final discussion point, we comment on how the dependencies in equation (12) may be leveraged to identify methods for mitigating this facility effect. In this context, mitigation means the thruster's coupling voltage is rendered insensitive to facility pressure such that parametric studies of coupling voltage (figure 4) would yield a horizontal line. We in turn would be confident that the measured value in the facility would be representative of an on-orbit value.

Reviewing the model parameters in equation (12), we see that $\bar{P}_{\mathrm{T}}$ depends linearly on the plasma density originating from the thruster. If for a given operating condition, this density could be raised, then the sensitivity of the model to facility pressure would be weaker. One possible method for achieving this end is to artificially increase the plasma density in the near field. This could be accomplished by raising the flow fraction of gas through the cathode, for example, or with an auxiliary injector mounted on the thruster. Such a method has recently been explored in the work by Cusson *et al* [26] in the context of mitigating another facility effect—the movement of acceleration zone with pressure. With that said, while in principle this method may help reduce the sensitivity of the cathode coupling voltage, the benefits gained by the reduced risk for the ground to flight transition must be weighed against the wasted propellant devoted to this mitigation method.

7. Conclusion

In this work, we have derived an analytical model for the dependence of the cathode coupling voltage in a Hall thruster on facility pressure. We arrived at this result from a generalized Ohm's law for the electron dynamics subject to a number of simplifying assumptions informed by recent experimental measurements. Most notably, we assumed that the electron current primarily flows along magnetic field lines in the near-field of the cathode plume, that the electron collision frequency is non-classical, and that downstream of the main cathode plume, the thruster electron dynamics are approximately Boltzmann. We have shown there are two contributions to the coupling voltage that depend on facility pressure: a Boltzmann effect that leads to worsening in cathode coupling with pressure and a resistive-driven term that has the opposite effect. The final result we have derived has three model parameters that must be inferred from data.

We have applied the new model to 12 different thruster configurations and operating conditions and shown that it can match—within experimental uncertainty—measured trends in coupling voltage. We similarly have quantified our confidence

in each model prediction through the lens of Bayesian inference. This approach has allowed us to incorporate physical intuition about the appropriate bounds for the model parameters as well as to quantify explicitly the impact of experimental uncertainty. Most notably, we have demonstrated that while it is possible to extrapolate to on-orbit conditions with the model, the confidence in these extrapolations is directly linked to the uncertainty in ground-based measurements.

We have discussed in this work the limitations of our underlying assumptions and as well as their physical significance. We in turn have used our physics-based model to interpret the impact of cathode placement on the coupling voltage, to identify how the model may be used to project the impact of coupling voltage on overall thruster performance when transitioning from ground to space, and to motivate potential techniques for reducing the coupling voltage's sensitivity to pressure. We also examined our result in the context of previous studies that have derived similar models for coupling voltage, outlining key similarities and differences that stem from the underlying assumptions.

Ultimately, this work has been motivated by a need to address a major challenge in the field of electric propulsion: how to translate ground tests to an on-orbit environment. Our approach here complements the current practice of systematically decreasing facility pressure to the lowest value supported by a facility and then using a best-fit function to the data to extrapolate to space-like conditions. By rooting the function used to extrapolate the data in a first-principles analysis and applying rigorous Bayesian inference, we are able to increase confidence in the projections of cathode coupling voltage to orbit. This combination of physics-based, data-driven analysis may serve as a future template to address other outstanding facility related effects.

Acknowledgments

Appendix A

We draw examples from previous experimental studies to justify the assumption outlined in section 2.5 that the coefficients $c_1, c_2 \ll 1$. In reference [42], the typical coupling length was found to be $L \approx 5$ cm (inferred from the plume lengthscale), while cathode orifice radii typically range from 2–5 mm. We therefore anticipate $L/r \sim \mathcal{O}[10]$. On the other hand, while the plasma density at the cathode orifice exit is the highest in the entire thruster geometry, $n_{e(0)} \sim 10^{20}$ m^{-3}, the background density of plasma from the facility and from the thruster plume near the cathode drop are orders of magnitude lower. For example, for a reference pressure of $P_{ref} = 10^{-5}$ Torr-xenon (a typical maximum working pressure) at room temperature, the corresponding neutral density is $P_{ref}/(k_B T_F) = 3.2 \times 10^{17}$ m^{-3}. Assuming a generous ionization fraction of $c' = 0.1$, we thus would find $c_2 \sim \mathcal{O}[10^{-2}]$. Working then under the assumption that $\mathcal{O}[c_1] = \mathcal{O}[c_2]$ and using our typical value of L/r, we can conclude that both coefficients are less than unity.

Appendix B

We show in this section the values plotted in figure 4 in tabular form.

SPT-100 (L3)			SPT-100 (Aerospace)		
P_b (μTorr)	V_{cc} (V)	V_{error} (V)	P_b (μTorr)	V_{cc} (V)	V_{error} (V)
1.67	31.20	0.3	3.45	31.12	0.3
4.11	31.95	0.3	4.27	31.29	0.3
6.97	32.02	0.3	8.04	31.89	0.3
12.3	32.84	0.3	14.4	32.30	0.3
15.8	32.83	0.3	24.9	33.11	0.3
25.1	33.09	0.3	49.1	32.46	0.3
38.2	32.58	0.3	73.7	32.13	0.3
55.1	32.10	0.3			

PPS 1350-G			H9		
P_b (μTorr)	V_{cc} (V)	V_{error} (V)	P_b (μTorr)	V_{cc} (V)	V_{error} (V)
3.9	32.67	0.2	7.1	24.99	0.5
7.9	33.27	0.2	12	25.96	2
13	33.33	0.2	16	26.65	0.5
26	33.69	0.2	21	26.97	0.5
37	33.67	0.2	26	27.55	0.5
54	34.38	0.2	30	27.94	0.5

BHT-1500 internal			BHT-1500 external		
P_b (μTorr)	V_{cc} (V)	V_{error} (V)	P_b (μTorr)	V_{cc} (V)	V_{error} (V)
4.2	14.98	0.2	4.8	28.41	0.2
8.8	15.46	0.2	10	28.03	0.2
30	16.14	0.2	30	26.13	0.2

NASA-173M ($Y = 0$)			NASA-173M ($Y = 6$)		
P_b (μTorr)	V_{cc} (V)	V_{error} (V)	P_b (μTorr)	V_{cc} (V)	V_{error} (V)
8.7	29.60	0.2	8.7	21.99	0.2
13	27.95	0.2	13	19.36	0.2
18	26.78	0.2	18	16.63	0.2
33	24.12	0.2	33	12.79	0.2

HiVHAc 300 V–3.0 kW			HiVHAc 500 V–3.0 kW		
P_b (μTorr)	V_{cc} (V)	V_{error} (V)	P_b (μTorr)	V_{cc} (V)	V_{error} (V)
1.9	23	1	1.9	40	1
5.6	20	1	5.6	33	1
19	18	1	9.4	27	1
			19	20	1

HERMeS 300 V–4.7 kW			HERMeS 500 V–12.5 kW		
P_b (μTorr)	V_{cc} (V)	V_{error} (V)	P_b (μTorr)	V_{cc} (V)	V_{error} (V)
4.0	18.9	4	5.3	19.1	4
6.0	19.5	4	8.0	19.3	4
7.8	19.8	4	10.6	19.4	4
11.6	20.1	4	15.5	20.0	4
19.1	21.0	4	28.9	21.1	4

ORCID iDs

B A Jorns ⬤ https://orcid.org/0000-0001-9296-2044
M P Byrne ⬤ https://orcid.org/0000-0001-5931-1581

References

[1] Biagioni L, Kim V, Nicolini D, Semenkin V and Wallace N C 2003 Basic issues in electric propulsion testing and the need for international standards *Proc. of the 28th Int. Electric Propulsion Conf., (IEPC-2003-230)*

[2] Randolph T, Kim V, Kaufman H, Kozubsky K, Zhurin V and Day M 1993 Facility effects on stationary plasma thruster testing *Proc. of the 23rd Int. Electric Propulsion Conf., (IEPC-1993-93)*

[3] Bugrova A I and Morozov A I 1995 Influence of vacuum conditions on the SPT operation *Proc. of the 24th Int. Electric Propulsion Conf., (IEPC-1995-046)*

[4] DeGrys K H, Tilley D L and Aadland R S 1999 BPT Hall thruster plume characteristics *Proc. of the 35th AIAA/ASME/SAE/ASEE Joint Propulsion Conf. and Exhibit, (AIAA-1999-2283)*

[5] Tilley D, De Grys K and Myers R 1999 Hall thruster-cathode coupling *Proc. of the 35th AIAA/ASME/SAE/ASEE Joint Propulsion Conf. and Exhibit, (AIAA-1999-2865)*

[6] Hofer R R, Peterson P and Gallimore A 2001 Effects of facility backpressure on the performance and plume of a Hall thruster *Proc. of the 27th Int. Electric Propulsion Conf., (IEPC-2001-045)*

[7] Mazouffre S, Pagnon D and Bonnet J 2004 Two ways to evaluate the Xe^+ ion flow velocity in a Hall effect thruster *Proc. of the 40th AIAA/ASME/SAE/ASEE Joint Propulsion Conf. and Exhibit, (AIAA-2004-3949)*

[8] Walker M L R, Victor A L, Hofer R R and Gallimore A D 2005 *J. Propul. Power* **21** 408–15

[9] Byers D and Dankanich J 2009 A review of facility effects on Hall effect thrusters *Proc. of the 31st Int. Electric Propulsion Conf., (IEPC-2009-076)*

[10] Peng E, Yu D and Jiang B 2009 Experimental investigation of backpressure effects on the ionization and acceleration processes in a Hall thruster *Proc. of the 31st Int. Electric Propulsion Conf., (IEPC-2009-119)*

[11] Brown D L and Gallimore A D 2011 *J. Propul. Power* **27** 573–85

[12] Nakles M R and Hargus W A 2011 *J. Propul. Power* **27** 737–43

[13] Hargus W, Tango L J and Nakles M R 2013 Background pressure effects on krypton Hall effect thruster internal acceleration *Proc. of the 33rd Int. Electric Propulsion Conf., (IEPC-2013-340)*

[14] Huang W, Kamhawi H and Haag T 2013 Effect of background pressure on the performance and plume of the HiVHAc Hall thruster *Proc. of the 33rd Int. Electric Propulsion Conf., (IEPC-2013-54)*

[15] Diamant K, Liang R and Corey R 2014 The effect of background pressure on SPT-100 Hall thruster performance *Proc. of the 50th AIAA/ASME/SAE/ASEE Joint Propulsion Conf., (AIAA-2014-3710)*

[16] Frieman J D, King S T, Walker M L R, Khayms V and King D 2014 *J. Propul. Power* **30** 1471–9

[17] Hofer R R and Anderson J R 2014 Finite pressure effects in magnetically shielded Hall thrusters *Proc. of the 50th AIAA/ASME/SAE/ASEE Joint Propulsion Conf., (AIAA-2014-3709)*

[18] Huang W, Kamhawi H, Lobbia R B and Brown D L 2014 Effect of background pressure on the plasma oscillation characteristics of the HiVHAc Hall thruster *Proc. of the 50th AIAA/ASME/SAE/ASEE Joint Propulsion Conf. 2014, (AIAA-2014-3708)*

[19] Spektor R, Tighe W G, Stoltz P H and Beckwith K R C 2015 Facility effects on Hall thruster performance through cathode coupling *Proc. of the 34th Int. Electric Propulsion Conf., (IEPC-2015-309)*

[20] Huang W, Kamhawi H, Haag T W, Lopez Ortega A and Mikellides I G 2016 Facility effect characterization test of NASA's HERMeS Hall thruster *Proc. of the 52nd AIAA/SAE/ASEE Joint Propulsion Conf., (AIAA-2016-4828)*

[21] Frieman J D, Walker J A, Walker M L R, Khayms V and King D Q 2016 *J. Propul. Power* **32** 251–64

[22] Spektor R, Tighe W G and Kamhawiz H 2016 Laser induced fluorescence measurements in a Hall thruster plume as a function of background pressure *Proc. of the 52nd AIAA/SAE/ASEE Joint Propulsion Conf., (AIAA-2016-4624)*

[23] Frieman J D, Liu T M and Walker M L R 2017 *J. Propul. Power* **33** 1087–101

[24] Dankanich J W, Walker M, Swiatek M W and Yim J T 2017 *J. Propul. Power* **33** 668–80

[25] Snyder J S, Lenguito G, Frieman J D, Haag T W and Mackey J A 2018 The effects of background pressure on SPT-140 Hall thruster performance *Proc. of the 54th AIAA/SAE/ASEE Joint Propulsion Conf., (AIAA-2018-4421)*

[26] Cusson S E, Byrne M P, Jorns B A and Gallimore A D 2019 Investigation into the use of cathode flow fraction to mitigate pressure-related facility effects on a magnetically shielded Hall thruster *Proc. of the AIAA Propulsion and Energy Forum and Exposition, (AIAA-2019-4077)*

[27] MacDonald-Tenenbaum N, Pratt Q, Nakles M, Pilgram N, Holmes M and Hargus W 2019 *J. Propul. Power* **35** 403–12

[28] Kamhawi H, Huang W, Haag T, Yim J and Herman D 2019 Characterization tests of NASA's Hall effect rocket with magnetic shielding thruster *Proc. of the 52nd AIAA/SAE/ASEE Joint Propulsion Conf., (AIAA-2016-4826)*

[29] Cusson S E, Dale E T, Jorns B A and Gallimore A D 2019 *Phys. Plasmas* **26** 023506

[30] Byrne M P and Jorns B A 2019 Data-driven models for the effects of background pressure on the operation of Hall thrusters *Proc. of the 36th Int. Electric Propulsion Conf., (IEPC-2019-630)*

[31] Mikellides I G, Lopez Ortega A, Chaplin V H and Snyder J S 2020 *Plasma Sources Sci. Technol.* **29** 035010

[32] Lopez Ortega A, Mikellides I G, Chaplin V H, Snyder J S and Lenguito G 2020 *Plasma Sources Sci. Technol.* **29** 035011

[33] Cusson S E, Jorns B A and Gallimore A D 2017 Simple model for cathode coupling voltage versus background pressure in a Hall thruster *Proc. of the 53rd AIAA/SAE/ASEE Joint Propulsion Conf., AIAA-2017-4889* (Atlanta, GA)

[34] Goebel D M, Jameson K K, Katz I and Mikellides I G 2007 *Phys. Plasmas* **14** 1–15

[35] Mikellides I G, Katz I, Goebel D M and Jameson K K 2007 *J. Appl. Phys.* **101** 063301

[36] Jorns B A, Mikellides I G and Goebel D M 2014 *Phys. Rev. E* **90** 1–10

[37] Jorns B A, Dodson C, Goebel D M and Wirz R 2017 *Phys. Rev. E* **96** 023208

[38] Lopez Ortega A and Mikellides I G 2016 *Phys. Plasmas* **23** 043515

[39] Sary G, Garrigues L and Boeuf J-P 2017 *Plasma Sources Sci. Technol.* **26** 055007

[40] Sary G, Garrigues L and Boeuf J-P 2017 *Plasma Sources Sci. Technol.* **26** 055008

[41] Ortega A L, Jorns B A and Mikellides I G 2018 *J. Propul. Power* **34** 1026–38

[42] Jorns B A, Cusson S E, Brown Z and Dale E 2020 *Phys. Plasmas* **27** 022311

[43] Mikellides I G, Lopez Ortega A, Goebel D M and Becatti G 2020 *Plasma Sources Sci. Technol.* **29** 035003

[44] Goebel D M and Katz I 2008 *Fundamentals of Electric Propulsion: Ion and Hall Thrusters* (New York: Wiley)

[45] Hofer R R 2004 Development and characterization of high-efficiency, high-specific impulse xenon Hall thrusters *PhD Dissertation* University of Michigan

[46] Boyd I D 2001 *J. Spacecr. Rockets* **38** 381–7

[47] Mikellides I G, Goebel D M, Jorns B A, Polk J E and Guerrero P 2015 *IEEE Trans. Plasma Sci.* **43** 173–84

[48] Sivia D and Skilling J 2006 *Data Analysis: A Bayesian Tutorial* (Oxford: Oxford University Press)

[49] Skilling J 2006 *Bayesian Anal.* **1** 833–59

[50] Walker M L R 2005 Effects of facility backpressure on the performance and plume of a Hall thruster *PhD Dissertation* University of Michigan

[51] Matlock T S, Nakles M R and Spektor R 2017 Pressure dependence of near-field plume properties in a 1 kW laboratory Hall thruster *Proc. of the 35th Int. Electric Propulsion Conf., (IEPC-2017-20)*

[52] Diamant K D, Lee T, Liang R, Noland J, Vial V and Cornu N 2016 Performance and plume characterization of the PPS 1350-G Hall thruster *Proc. of the 52nd AIAA/SAE/ASEE Joint Propulsion Conf., (AIAA-2016-4543)*

[53] Diamant K D, Curtiss T, Spektor R, Beiting E, Hruby V, Pote B, Kolenick J and Paintal S 2015 Performance and plume characterization of the BHT-1500 Hall thruster *Proc. of the 34th Int. Electric Propulsion Conf., (IEPC-2015-69)* (Hyogo-Kobe, Japan)

[54] Cusson S E 2019 Impact of neutral density on the operation of high-power magnetically shielded Hall thrusters *PhD Dissertation* University of Michigan

[55] Tighe W, Spektor R, Diamant K and Kamhawi H 2015 Effects of background pressure on the NASA 173M Hall current thruster performance *Proc. of the 34th Int. Electric Propulsion Conf., (IEPC-2015-152)*